University of Nebraska - Lincoln

DigitalCommons@University of Nebraska - Lincoln

Faculty Publications, Department of Physics and Astronomy

Research Papers in Physics and Astronomy

2017

The lattice stiffening transition in UO2 single crystals

Christopher Young

James Petrosky

J. Matthew Mann

Eric M. Hunt

David Turner

See next page for additional authors

Follow this and additional works at: https://digitalcommons.unl.edu/physicsfacpub

Authors

Christopher Young, James Petrosky, J. Matthew Mann, Eric M. Hunt, David Turner, and Peter A. Dowben

The lattice stiffening transition in UO$_2$ single crystals

Christopher Young[1], James Petrosky[1], J Matthew Mann[2], Eric M Hunt[2], David Turner[2,3] and Peter A Dowben[4]

[1] Department of Engineering Physics, Air Force Institute of Technology, 2950 Hobson Way, Wright-Patterson Air Force Base, OH 45433-7765, USA
[2] Air Force Research Laboratory, Wright-Patterson Air Force Base, OH 45433-7765, USA
[3] Oak Ridge Institute for Science and Education, Oak Ridge, TN, USA
[4] Department of Physics and Astronomy, Theodore Jorgensen Hall, 855 North 16th Street, University of Nebraska-Lincoln, Lincoln, NE 68588-0299, USA

E-mail: james.petrosky@afit.edu

Abstract
The effective Debye temperatures (Θ_{DE}) of the surface region of UO$_2$ single crystals, prepared by the hydrothermal synthesis technique, were obtained from temperature-dependent x-ray photoemission in the temperature range of 300 K–623 K. A lattice stiffening transition, characterized by different regions of different effective Debye temperature, 500 ± 59 K below 475 K and 165 ± 21 K above 475 K is identified. A comparison of the temperature dependence of the effective UO$_2$ Debye temperature, with the changes in the lattice expansion coefficient for UO$_2$, support strong lattice-phonon interaction arising from the Jahn–Teller distortion.

Keywords: UO$_2$, XPS, Jahn–Teller distortions, Debye temperature

S Online supplementary data available from stacks.iop.org/JPhysCM/29/035005/mmedia

(Some figures may appear in colour only in the online journal)

1. Introduction

Uranium oxide is commonly used in the nuclear industry and thus its mechanical properties are of great interest. While recent ultrafast hopping dynamics studies of UO$_2$ by femtosecond pump–probe spectroscopy [1] suggest no Jahn–Teller distortions in this system, the Jahn–Teller distorted structure, with an oxygen displacement along the $\langle 1\,1\,1 \rangle$ direction is considered more stable [2]. Distortions and volume changes, however, are also associated with the creation of point defects on which there has been considerable effort in the case of UO$_2$ [2–14]. While defect creation is expected to occur at high(er) temperatures, especially above 1000–2000 K, the simplified phase diagram of the UO$_x$ system [15, 16] suggests a UO$_{2+x}$ to UO$_{2+x}$ and U$_4$O$_{9-y}$ transition between 473 K and 670 K. Such a structural phase transition would alter the density of lattice imperfection and a change in defect density would enhance Jahn–Teller distortions significantly [2]. Yet, nonlinearities are seen in

the thermal expansion coefficient in the region of 500 K [17]. This variation in the thermal expansion coefficient is either related to defect creation or anharmonic distortions as would occur with enhanced Jahn–Teller distortions [18–21] and would be associated with a pronounced change in the Debye–Waller factors.

The effective Debye temperature is, in some sense, an indication of the lattice stiffness, with organic 'soft' materials systems exhibiting Debye temperatures in the region of 50 K [22], while a Debye temperature of several hundred K is more typical of a transition metal surface [23]. Thus dramatic changes in the Debye temperature are a typical signature of a change in lattice 'stiffness' and a lattice stiffness transition. Assessment of the Debye Waller factors, as a function of temperature, then may provide insight as to whether there is [2, 19, 20] or is not [1] a significant role for enhanced Jahn–Teller distortions in UO$_2$, as might result in a distortion of the lattice, as suggested for UO$_2$ [24], a change in volume, or a change in lattice 'stiffness'.

2. Material and methods

2.1. Synthesis of materials

The UO$_2$ crystals were prepared by hydrothermal synthesis. This employed an aqueous growth reaction nutrient solution of high-purity (99.998% UO$_2$, International Bioanalytical Laboratories, Lot# B206093), depleted uranium dioxide powder and a 6 M cesium fluoride mineralizer (99.9% CsF, Alfa Aesar, Lot #S25A038) to aid solubility. The reaction was contained in a sealed silver ampule (99.95% Ag, Refining Systems, Inc.) which was held at growth conditions in an autoclave for 45 days at a pressure of 20 kpsi. The growth and dissolution regions of the autoclave were maintained at 600 °C and 650 °C, respectively, which provided a temperature gradient of 50 °C between the growth and dissolution zones. The resulting crystal was highly faceted with macroscopically smooth faces and measured approximately $2 \times 3 \times 2$ mm.

2.2. Physical characterization

Single crystal x-ray diffraction (XRD) measurements yield a lattice constant of 5.4703 ± 0.0006 Å for crystals produced under these growth conditions indicating a stoichiometry of UO$_{2.003}$ [15, 25]. X-ray fluorescence (XRF) analysis indicated the crystal was of high purity (see supplementary materials (stacks.iop.org/JPhysCM/29/035005/mmedia)).

The sample was placed under high vacuum (10^{-9} Torr) and annealed and sputtered with 1 kV Ar$^+$ ions. The sample was subsequently annealed *in vacuo* at 623 K for 12 h. X-ray photoemission spectroscopy (XPS) confirmed the adventitious carbon intensity was less than 3% of the U $4f_{7/2}$ peak. The photoemission experiments utilized a VG Scienta R3000 electron analyzer and a Specs XR50 x-ray source, providing Mg Kα radiation at 1253.6 eV. The photoelectrons were collected normal to the sample surface, in the analyzer geometry used here, while the x-ray source was offset from the normal at a fixed 45° angle. The spectral intensity was computed from the average of 5 measurements, using a pass energy of 100 eV and a constant x-ray power output, and then repeated at 14 different temperatures. To ensure a more accurate assessment of temperature, spectra were taken as the temperature was increased, and the sample allowed to stabilize at the measurement temperature for an hour. The x-ray source and the analyzer are held in a constant flux and constant detection mode. For a well characterized electron energy analyzer, like that used here, this means that any change in count rate is the result of a change in the photoelectron generation rate. Since the measurements are done for increasing temperature, not decreasing temperature, mechanical fluctuations are minimized, and the sample geometry is fixed. Were there some time dependent variation in detector efficiency, then reproducibility would be absent from experiment to experiment. This is clearly not the case.

3. The effective Debye temperature

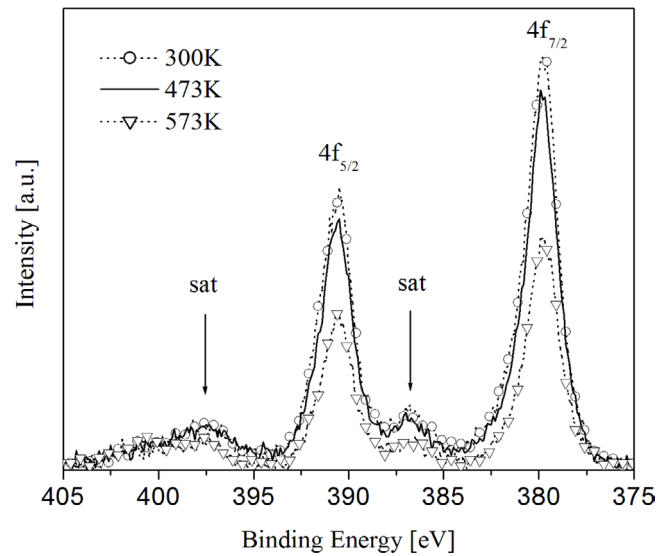The U $4f$ spectra, shown in figure 1, are very temperature dependent. The measured photoemission binding energies

Figure 1. The XPS core level spectra in the region of the U $4f$, with the typical $E^{-1/2}$ background subtracted. Data for three temperatures are shown, indicating a sharp decline of U $4f$ core level photoemission intensity with increasing temperature. The characteristic satellite peaks of UO$_2$ are clearly visible.

(denoted as $E_F - E$), U $4f_{7/2}$ at 380.1 ± 0.1 eV and U $4f_{5/2}$ at 390.9 ± 0.1 eV are consistent with the binding energies of U $4f_{7/2}$ at 380.8 ± 0.2 eV and U $4f_{5/2}$ at 391.7 ± 0.2 eV [26] and U $4f_{7/2}$ at 380.0 eV and U $4f_{5/2}$ at 390.8 eV [27] reported previously. The prior work [26, 27] exhibits the same $4f$ 'shake-up' peaks or satellite features, located $\approx$7 eV higher binding energy, seen here (figure 1) at 386.7 ± 0.1 eV and 397.4 ± 0.1 eV, a characteristic feature of UO$_2$ $4f$ photoemission spectra. The 10.8 eV value of the spin–orbit coupling is in excellent agreement to that of [27] and within the experimental uncertainty of [26].

While the true surface Debye temperature, containing the in-plane and anharmonic motions, is difficult to measure in most surface spectroscopies [23], the effective surface Debye temperature can be readily obtained using low-energy electron diffraction (LEED), x-ray photoelectron spectroscopy, electron energy loss spectroscopy (EELS), inverse photoemission spectroscopy (IPES), and other surface sensitive techniques [22, 23, 28–37]. Since the intensity of an emitted or scattered electron beam exponentially decays, with increasing temperature, due to increases in the thermal vibration, we can calculate the surface Debye temperature Θ_{DE} with careful analysis of the intensity change as a function of temperature [23, 28, 29, 35–37]:

$$I = I_0 e^{-2W} \text{ where } 2W = \frac{3\hbar^2(\Delta k)^2}{2mk_B(\Theta_{DE})^2} T \tag{1}$$

where W is the Debye–Waller factor, T is the temperature of the sample (in Kelvin), $\hbar\Delta k$ is electron momentum transfer, m is the mass of the scattering center (^{238}U atom), k_B is Boltzman's constant, T is the absolute temperature, and Θ_{DE} is the effective surface Debye temperature. The Debye–Waller factor has been computed from the slope of the natural logarithmic ratio of the core-level photoemission intensities, as a function of temperature, as seen in figure 2, using the kinetic
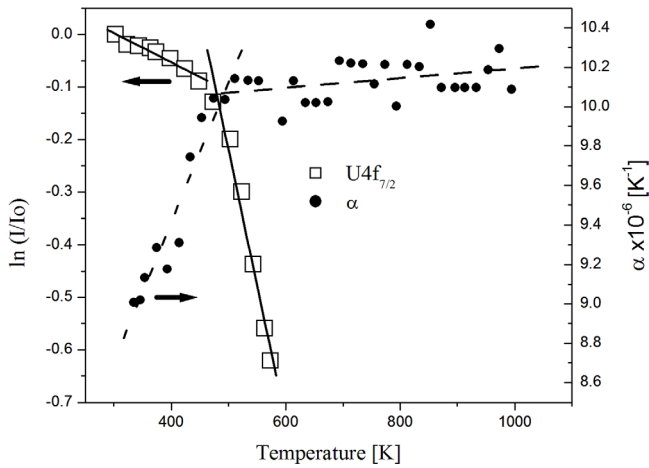
Figure 2. The natural logarithmic ratio of U $4f_{7/2}$ (kinetic energy 870 eV) photoemission intensities compared to the linear expansion coefficient, α, for UO_2 as adapted from [17]. The XPS data shows two distinct regions of linearity; 300–450 K ($\Theta_{DE} = 500 \pm 59$ K) and 470–600 K ($\Theta_{DE} = 165 \pm 21$ K). The abrupt change, between 476 K and 486 K, suggests the lattice stiffening transition and is in good agreement with the change in α observed at ~490 K. The horizontal arrows indicate the appropriate vertical axis scale.

energy of the photoemission features to estimate $\hbar\Delta k$ [23, 35–38]. Because the temperature dependence of the various U core level were used, the effective Debye temperature measured in this manner is strongly weighted for U, and defined as the scattering center in equation (1), as has been done in other compound systems [30, 38]. While the effective Debye temperature of equation (1) does not generally include anharmonic contributions [23, 28, 29, 35, 37, 38], it is a characteristic signature of motion along the surface normal in the region of the surface because of the very short photoelectron mean free path.

As seen in figure 2, the data shows two distinct regions of linearity for the decrease in the uranium core level photoemission intensities; 300–450 K and 470–600 K. The intersection of the linear fit lines (figure 2) marks the threshold temperature at which the measured effective Debye temperature undergoes an abrupt change, roughly between 476 K and 486 K based on the U $4f_{7/2}$ peak. The slope of the fitting, above and below the threshold temperature, equates to a transition from a high effective Debye temperature Θ_{DE} to a low effective Debye temperature, i.e. from 500 ± 59 K below 475 K to 165 ± 21 K above 475 K. These values are in rough agreement with previous bulk crystal estimates, with the higher value of 500 ± 59 K for the Debye temperature corresponding to a value of ~616 K [20]. This is also supported by a measured 523 ± 33 K obtained by using the higher kinetic energy U $5f$ shell. The lower value Debye temperature of 165 ± 21 K, seen above 475 K, corresponding to 182 K reported in [21]. While the effective Debye temperature extracted from XPS measurements are expected to be largely from the surface region, this depends on the photoelectron mean free path to some extent [37]. It is not uncommon for surface and bulk Debye temperatures to differ based on the lower coordination of the surface
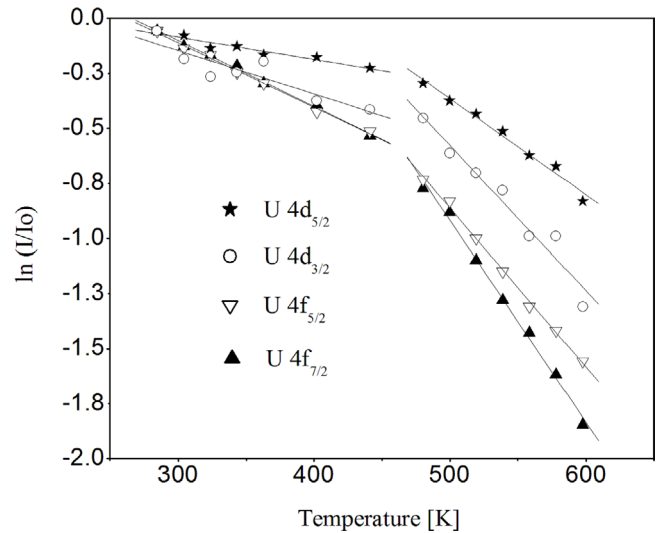

Figure 3. The natural logarithmic ratio of normalized intensities for the uranium $4f$ and $4d$ core level photoemission peaks as a function of temperature. The data is obtained for samples not annealed after cold sputter cleaning of the surface. The higher U $4f$ photo-electron energies (870 and 859 eV) indicate a lower effective Debye temperature than the U $4d$ peaks (512 and 468 eV). In both cases, the change in effective Debye temperature is marked by a sharp change in the rate of the decrease in intensity, with increasing temperature, near 480–490 K.

atom bonding at the surface versus the bulk [23, 28, 29, 32, 33, 35, 38]. The expectation, based on very simple models [28, 29, 33], is that the effective surface Debye temperature is 2/3 the bulk Debye temperature, but this difference, between the surface and the bulk varies considerably. In spite of these complexities, the stark transition between two regions of constant effective Debye temperature is unexpected and suggests some sort of lattice stiffening transition.

4. Persistent Jahn–Teller distortions

Other lattice stiffening transitions, corresponding to a significant change Debye temperature Θ_{DE}, are known. These have been attributed to dynamic Jahn–Teller distortions associated with orbital rehybridization and a nonmetal to metal transition [18, 19], dipole–dipole coupling in a polymer ferroelectric [39], and an order–disorder transition [36, 37]. The regions of constant Θ_{DE} intersect near the point at which the lattice expansion coefficient shows a marked change for UO_2 [17], within the margin of experimental error. This is more akin to the dynamic Jahn–Teller distortion driven lattice stiffening transition in the cubic perovskites [18, 19] than an order-to-disorder transition that might be associated with a sudden and abrupt change in defect density.

A comparison of the effective Debye temperature transition, derived from the XPS data, with the phase diagram [15, 16] suggests that the ($UO_{2+x} + U_4O_{9-y}$) phase presents a stiffer surface lattice than the (UO_{2+x}) phase. The U_4O_9 mixed-oxide structure is associated with charge-compensation of the addition of oxygen to the UO_2 fluorite structure.

Oxygen defects are added to the fluorite structure of UO_2 until the mixed-oxide structure forms. This U_4O_{9-y} structure is essentially the oxygen-defected UO_{2+x} fluorite structure. It is somewhat surprising that this would be the stiffer analysis, given the expectation of a high defect density.

We have studied less annealed samples, still rich in defects from Ar^+ sputtering, the results of which are summarized in figure 3. In contrast to the effective Debye temperature of 500 ± 59 K below 475 K for the well annealed sample, the defect rich UO_2 surface displays a lower effective Debye temperature of 230 ± 44 K based on the temperature dependence of the U $4f_{7/2}$ core level feature, in x-ray photoemission. Similar effective Debye temperature values of 285 ± 30 K were obtained from the U $4d$ core level. The kinetic energy of the photoelectrons from the U $4f$ levels is large, approximately 859 eV and 870 eV, so should be more representative of the bulk [38], so the defects, introduced by Ar^+ bombardment, must persist well into the bulk, i.e. deeper into a selvedge region below the surface. For the 'softer' high temperature phase, above 475–500 K, the measured effective Debye temperature decreases from 165 ± 21 K (for the well annealed sample) to 128 ± 15 K and 138 ± 15 K, as obtained from the U $4f$ and U $4d$ levels respectively. But, as seen in figure 3, all data sets indicate a stiffening of the lattice, apparent from the change in the effective Debye temperature, in the vicinity of 475 K, consistent with the change in Debye temperature measured on the well annealed and less defective UO_2 surface (figure 2).

5. Conclusions

The correlation of changing Debye–Waller factors and discontinuity in the thermal expansion coefficient, as seen in figure 2, points to a significant role of Jahn–Teller distortions, as suggested in [2]. Whether these Jahn–Teller distortion amplitudes are due to defects, as suggested by the phase diagram, or $5f$ rehybridization, cannot be determined from this data. We find that defect density does have a profound effect on the effective Debye temperature, but does not suppress the lattice stiffening transition seen between 470 and 510 K in UO_2.

Acknowledgments

References

[1] An Y Q, Taylor A J, Conradson S D, Trugman S A, Durakiewicz T and Rodriguez G 2011 *Phys. Rev. Lett.* **106** 207402
[2] Dorado B, Jomard G, Freyss M and Bertolus M 2010 *Phys. Rev.* B **82** 035114
[3] Nerikar P, Watanabe T, Tulenko J S, Phillpot S R and Sinnott S B 2009 *J. Nucl. Mater.* **384** 61–9
[4] Gupta F, Brillant G and Pasturel A 2007 *Phil. Mag.* **87** 2561–9
[5] Iwasawa M, Chen Y, Kaneta Y, Ohnuma T, Geng H Y and Kinoshita M 2006 *Mater. Trans.* **47** 2651–7
[6] Matzke H 1990 *J. Chem. Soc. Faraday Trans.* **86** 1243–56
[7] Chasanov M G, Leibowitz L and Gablenick S D 19734 *J. Nucl. Mater.* **49** 129
[8] Szwarc R 1969 *J. Phys. Chem. Solids* **30** 705
[9] Kerrisk J F and Clifton D G 1972 *Nucl. Technol.* **16** 531
[10] Hein R A, Sjodahl L H and Szwarc R J 1968 *J. Nucl. Mater.* **25** 99
[11] Browning P 1981 *J. Nucl. Mater.* **98** 345–56
[12] Harding J H, Masri P and Stoneham A M 1980 *Theoretical Physics Report* TP827 AERE
[13] Hyland G J and Ralph J 1983 *High Temp. High Press.* **15** 179–90
[14] Ronchi C and Hyland G J 1994 *J. Alloys Compd.* **213/4** 159–68
[15] Lynds L, Young W, Mohl J and Libowitz G 1963 *Nonstoichiometric Compounds* (Washington, DC: American Chemical Society) pp 58–65
[16] Kim D J, Kim J H, Kim K S, Yang J H, Kim S K and Koo Y H 2015 *J. Nucl. Sci. Technol.* **5** 102–6
[17] Ruello P, Desgranges L, Baldinozzi G, Calvarin G, Hansen T, Petot-Ervas G and Petot C 2005 *J. Phys. Chem. Solids* **66** 823–31
[18] Dai P, Zhang J, Mook H A, Foong F, Liou S H, Dowben P A and Plummer E W 1996 *Solid State Commun.* **100** 865–9
[19] Dai P, Zhang J, Mook H A, Liou S H, Dowben P A and Plummer E W 1996 *Phys. Rev.* B **54** R3694–7
[20] Dolling G, Cowley R A and Woods A D B 1965 *Can. J. Phys.* **43** 1397
[21] IAEA 1965 *Thermodynamic and Transport Properties of Uranium Dioxide and Related Phases, Report No 39* (Vienna: IAEA)
[22] Borca C N, Choi J, Adenwalla S, Ducharme S, Dowben P A, Robertson L, Fridkin V M, Palto S P and Petukhova N 1999 *Appl. Phys. Lett.* **74** 347–9
[23] Waldfried C, McIlroy D N, Zhang J, Dowben P A, Katrich G A and Plummer E W 1996 *Surf. Sci.* **363** 296–302
[24] Gofryk K *et al* 2014 *Nat. Commun.* **5** 4551
[25] Leinders G, Cardinels T, Binnemans K and Verwerft M 2015 *J. Nucl. Mater.* **459** 135–42
[26] Teterin Y A, Kulakov V M, Baev A S, Nevzorov N B, Melnikov I V, Streltsov V A, Masirov L G, Suglobov D N and Zelnekov A G 1981 *Phys. Chem. Miner.* **7** 151–8
[27] Van den Berghe S, Miserque F, Gouder T, Gaudreau B and Verwerft M 2001 *J. Nucl. Mater.* **294** 168–74
[28] Van Hove M A, Weinberg W H, Chan C M 1986 *Low-Energy Electron Diffraction: Experiment, Theory, and Surface Structure Determination* vol 6 (New York: Springer) p 134
[29] Clarke L J 1985 *Surface Crystallography* (New York: Wiley)

[30] Borca C N, Ristoiu D, Komesu T, Jeong H-K, Hordequin C, Pierre J, Nozieres J P and Dowben P A 2000 *Appl. Phys. Lett.* **77** 88–90

[31] Borca C N, Xu B, Komesu T, Jeong H-K, Liu M T, Liou S H and Dowben P A 2002 *Surf. Sci. Lett.* **512** L346

[32] Tonner B P, Li H, Robrecht M J, Chou Y C, Onellion M and Erskine J L 1986 *Phys. Rev.* B **34** 4386

[33] Kevan S D and Shirley D A 1980 *Phys. Rev.* B **22** 542

[34] Williams R S, Wehner P S, Stöhr J and Shirley D A 1977 *Phys. Rev. Lett.* **39** 302

[35] Hufner S 2003 *Photoelectron Spectroscopy, Principles and Applications* 3rd edn (Heidelberg: Springer)

[36] Losovyj Y B, Yakovkin I N, Jeong H-K, Wisbey D and Dowben P A 2004 *J. Phys.: Condens. Matter* **16** 4711–24

[37] Fukutani K, Lozova N, Zuber S M, Dowben P A and Losovyj Y B 2010 *Appl. Surf. Sci.* **256** 4796–800

[38] Jeong H-K, Komesu T, Dowben P A, Schultz B D and Palmstrøm C J 2002 *Phys. Lett.* A **302** 217–23

[39] Borca C N *et al* 1999 *Phys. Rev. Lett.* **83** 4562–5